Volume 10, Issue 3, 2020, 5472 - 5477 ISSN 2069-5837
Biointerface Research in Applied Chemistry
www.BiointerfaceResearch.com
https://doi.org/10.33263/BRIAC103.472477
Original Research Article Open Access Journal
Received: 17.02.2020 / Revised: 07.03.2020 / Accepted: 08.03.2020 / Published on-line: 12.03.2020

Identification of potential inhibitors for Bruton's Tyrosine Kinase (BTK) based on pharmacophore-based virtual screening

Muhammad Arba [1,*], **Oktovia Nurmawati** [1]
[1]Faculty of Pharmacy, Universitas Halu Oleo, Kendari, Indonesia, 93232
*corresponding author e-mail address: ***muh.arba@uho.ac.id*** | Scopus ID 57155296400

ABSTRACT
Bruton's tyrosine kinase (BTK) is well known for its role in the development, differentiation and proliferation of B-lineage cells. The dysregulation of BTK is closely related with the immunological disorders and BTK targeting is commonly studied in the treatment of immunological disorders. Here pharmacophore model was developed, and screening against ZINC database retrieved 1337 hit molecules of potential BTK inhibitors. Molecular docking was performed for all molecules and analysis on the top docked molecules revealed that the ligands interacted well in the binding pocket of BTK. A 100-ns molecular dynamics simulation confirmed the docked pose of ligand, while the calculation of binding free energy indicated that the hit molecule has comparable affinity with native ligand of BTK (2V3).
Keywords: *pharmacophore modeling; Bruton's tyrosine kinase (BTK); virtual screening; molecular docking; MM-PBSA.*

1. INTRODUCTION

Bruton's tyrosine kinase (BTK), a key member of the TEC family of cytoplasmic non-receptor protein tyrosine kinases, is well known for its role in the development, differentiation and proliferation of B-lineage cells [1,2]. BTK is widely found in hematopoietic cells and not found in natural killer or T cells [3,4]. The deregulation of BTK is closely related with the numerous B-cell-derived malignancies such as non-/hodgkin's lymphoma (NHL), systemic lupus, multiple sclerosis, B-cell lymphomas and leukemias [1]. Hence, BTK targeting is commonly studied in the treatment of immunological disorders.

Since the discovery of BTK in 1990, targeting BTK kinase has led to the finding of several BTK inhibitors both reversible and covalent irreversible, which were shown to be efficacious in the suppression of hematological malignancies. They include Ibrutinib, which was approved in 2013 for treating Chronic Lymphocytic Leukemia (CLL, the commonly found leukimia in Western countries), mantle cell lymphoma (MCL), and Waldenström's macroglobulinemia (WM) [3,5,6]. Other BTK inhibitors such as ONO-4059, CC-292, and acalabrutinib (Acerta Pharma BV, the Netherlands) are still in clinical tests for B-cell malignancies and autoimmune disorders treatments [7–10].
It is well known that the finding of new molecules with improved drug efficacy require a large amount of resources of both time and cost.

The approach of computer-aided drug design is promising tools to initiate the search for new lead molecules as it offers time and cost efficiency. Trustworthy molecule models can figure out the important characteristics of molecule that may affect the inhibitory activity of protein target [11]. However, in term of BTK inhibitor, computer-aided drug design approaches have been less applied.

The main aim of this study was to perform molecular modeling study based on pharmacophore model analysis to identify molecular hits of BTK inhibitors. Pharmacophore model was applied to screen for a new molecule of potential BTK inhibitors. The novel identified molecules were then subjected to molecular docking to reveal their binding modes of interaction.

2. MATERIALS AND METHODS

The pharmacophore model was generated using LigandScout Advanced 4.3 software [12]. The software provides a built-in set of pharmacophore features including hydrogen bond donor (HBD), hydrogen bond acceptor (HBD), positive ionizable area (PI), positive ionizable area (NI), hydrophobic interaction (H), aromatic ring (AR), metal binding location, and excluded volume. Structure of BTK complexed with 2V3 was used, taken from Protein Data Bank (www.rcsb.org) with the PDB ID 4OTR [13]. Screening against 159 actives and 8673 decoys downloaded from the Directory of Useful Decoys-Enhanced (DUD-E) [14] was conducted for model validation, while screening against ZINC database employing Pharmit (http://pharmit.csb.pitt.edu/) web server [15] was performed to retrieve potential hit molecules. Pharmit setting follows the default values.

Further, all hits were subjected to molecular docking simulation against BTK protein. Preparation of BTK structure was completed using AutoDockTools 1.5.6 [16]. The center for docking was plotted following the coordinates of BTK native ligand (2V3). Discovery Studio Visualizer 2016 was employed for analysis and visualization of docked poses

Molecular dynamics (MD) simulation for 100 ns was used to check the stability of docked pose of top docked ligand and native inhibitor (2V3), each complexed with BTK, employing AMBER16 package, the ff14SB force field [17] for protein, GAFF force field [18] and AM1-BCC [19] for ligands. The complex was

dissolved in a TIP3P water periodic cell with a 10 Å distance from the edge of the water box. Counterions were used to neutralize each system.

Multistage energy-minimization simulations were performed to relax sterical hindrance in each complex [20]. Further, temperature of system was gradually raised from 0 to 300 K in three sequential steps over 150 ps. The system was then subjected to equilibration at 300 K with a duration of 200 ps. The backbone heavy atoms were restrained in the equilibration steps. Finally, system was run for 100 ns in constant temperature and pressure ensemble employing pmemd.cuda module.

All hydrogen-involving bonds were constrained using SHAKE algorithm [21] with a time step of 0.002 ps. The particle-mesh Ewald algorithm (PME) was used to calculate electrostatics interactions [22] of a periodic box with radius cutoff for the Lennard-Jones (LJ) was set to 0.9 nm. The Langevin thermostat was used to control Langevin thermostat with a collision rate of 1.0 ps^{-1}. The snapshots were collected at an interval of 1 ps. The RMSD and RMSF were analyzed by CPPTRAJ module of AMBER16 [23], while visualization was conducted using the Visual Molecular Dynamics software [24]. Binding affinities were calculated for 15000 last frames of MD by following our previous work [25].

3. RESULTS

The model of pharmacophore was built using 2V3 structure. Molecular features involving hydrophobic interactions, hbond acceptor, and hbond donors were selected while generating the pharmacophore model. Figure 1 shows the features of pharmacophore BTK-2V3 interaction.

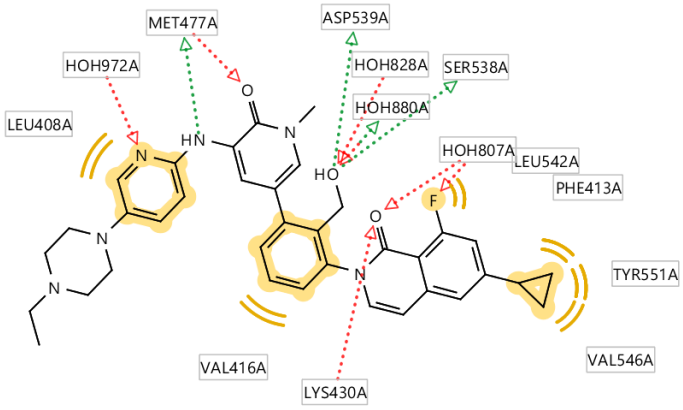

Figure 1. The features of pharmacophore.

Interaction of 2V3 with BTK consisted of four hydrophobics, seven hbond acceptors, and four hbond donors. Hypotheses were then built by combining those features, which gave 5 good models as indicated by their $AUC_{100\%}$ values and Goodness of hit (GH) scores. Table 1 shows five models of pharmacophore.

Among the five model above, four models, i.e. 2V3-1, 2V3-2, 2V3-3, and 2V3-4, had Goodness of hit-list (GH) score less than 7. GH score is a criterion to evaluate the ability of model to differentiate actives from decoys which account for both true actives and true inactives. GH score was evaluated according to Braga and Andrade (2013) [26], i.e.:

$$GH = \left(\frac{4}{4}YA + \frac{1}{4}Se\right)Sp$$

In which, YA is yield of actives, *Se* is Sensitivity, and *Sp* is Specifity. GH score 0.7 or higher is widely considered as indicator that a model of pharmacophore is valid. Therefore, model 2V3-5 was acceptable. Table 2 shows the GH score calculation.

In addition, evaluation of the model was also based on the Area Under Curve (AUC) of ROC curve. ROC curve was plot between true positive versus false positive. On the other words, ROC curve report Sensitivity (*Se*) as function of Specifity (*1-Sp*). In ROC curve, a higher AUC value represents better model of pharmacophore, and the threshold of AUC value was considered to be 0.5. Therefore, model 2V3-5 was valid according to both GH score and AUC value. Figure 2 displays the pharmacophore model of 2V3-5 and ROC curve.

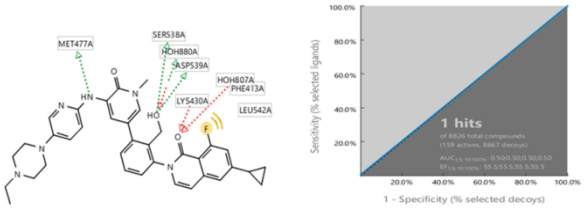

Figure 2. Best model of pharmacophore which consisted of three hydrogen bond acceptors (red dotted lines), three hydrogen bond donors (green dotted lines), and one hydrophobic (yellow sphere) features (left). The AUC of Receiver Operating Characteristic (ROC) curve (right).

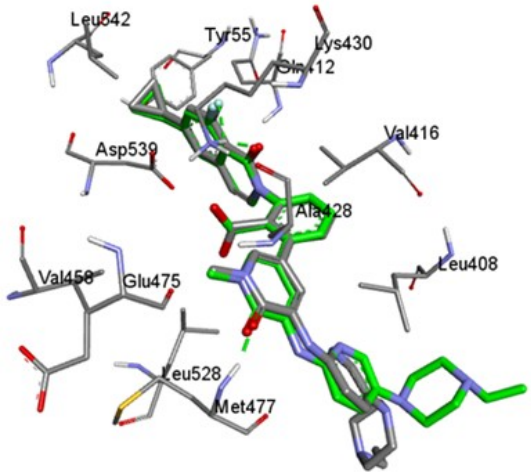

Figure 3. The superimposed 2V3 conformations of both experimental (grey) and docked (green) experiments.

Furthermore, screening for hit molecules against ZINC database retrieved 1337 hits. Molecular docking of all the 1337 hits gave binding energies with the values ranging from −4.13 to −10.90 kcal/mol. The binding energies were slightly higher than that of 2V3 (−12.68 kcal/mol). The docked pose of 2V3 with BTK was corroborated by hydrogen bonds (Hbonds) with Lys430 and Met477, while Asp539 was involved in C-hbond. Those residues were also observed in the x-ray pose of the ligand. Figure 3 shows both experimental and docked poses of 2V3.

Further analysis on the docked ligands resulted in four best docked hit molecules. They were Lig65/ZINC25044394 (E=−10.90 kcal/mol), Lig263/ZINC19583202 (E=−10.58 kcal/mol), Lig436/ZINC1704300257 (E=−10.38 kcal/mol), and

Lig380/ZINC257300426 (E=−10.15 kcal/mol). Figure 4 shows the 2D structures of four best docked hit molecules.

Table 1. Five good models of pharmacophore generated.

ID	Model of pharmacophore	Features	Goodness of hit (GH) score	$AUC_{100\%}$
2V3-1	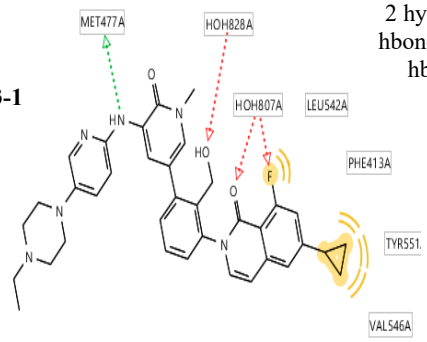	2 hydrophobics,3 hbond acceptors, 1 hbond donor	0.25	0.52
2V3-2	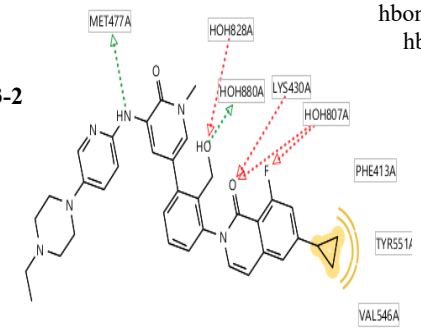	1 hydrophobic, 4 hbond acceptors, 2 hbond donors	0.12	0.50
2V3-3	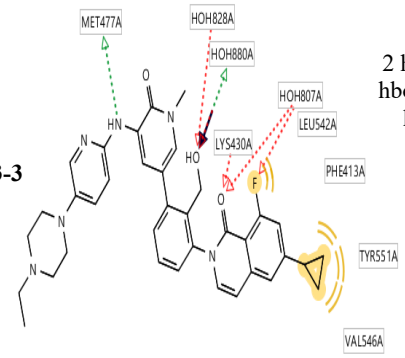	2 hydrophobics, 5 hbond acceptors, 2 hbond donors	0.18	0.50
2V3-4	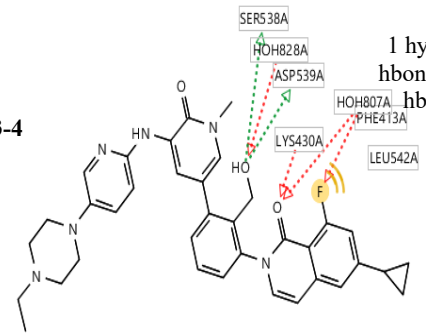	1 hydrophobic, 4 hbond acceptors, 2 hbond donors	0.50	0.50

2V3-5	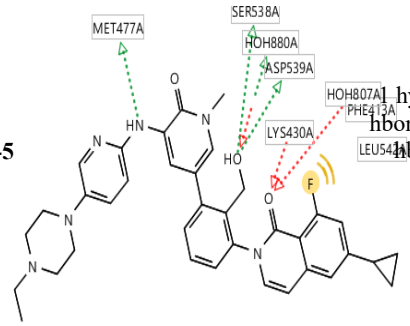 1 hydrophobic, 3 hbond acceptors, 4 hbond donors	0.75	0.50

Table 2. The GH score calculation.

Parameter	Value
Molecules in database (D)	8826
Active in database (A)	159
Obtained hits (Ht)	1
Active hits (Ha)	1
% actives [(Ha/Hit)*100]	100
% actives comparison [(Ha/A)*100]	0.628
Enrichment factor (E) [(Ha*D)/(Hit*A)]	55.509
False positives [Ht-Ha]	0
Goodness of Hit Score (GH)*	0.75

Table 3. Binding energies as predicted by MM-PBSA method.

Ligand	ΔE_{ELE} (kcal/mol)	ΔE_{VDW} (kcal/mol)	ΔE_{PBCAL} (kcal/mol)	ΔE_{PBSUR} (kcal/mol)	ΔE_{PBTOT} (kcal/mol)
2V3	−46.15±8.44	−67.87±3.75	86.99±6.20	−6.04±0.19	−33.07±7.99
Lig65/ZINC25044394	−0.68±1.92	−29.75±2.16	11.09±2.20	−2.61±0.12	−21.96±2.12

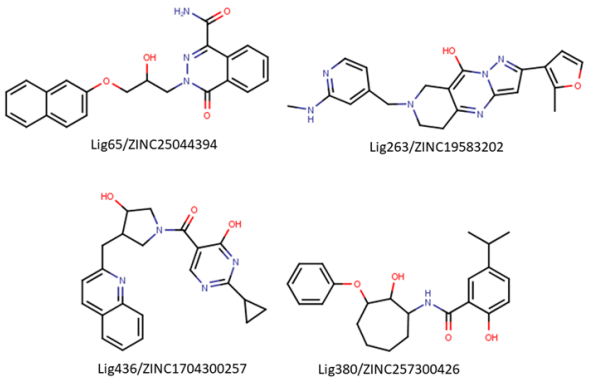

Figure 4. The structures of Lig65/ZINC25044394, Lig263/ZINC19583202, Lig436/ZINC1704300257, and Lig380/ZINC257300426.

Lig263/ZINC19583202 formed Hbond interactions with Lys430 through oxygen atoms of pyrimidine ring. Lig436/ZINC1704300257 also formed hbond with Lys430 through oxygen atoms of pyrimidine ring.

Lig380/ZINC257300426 also formed hbond with Lys430 through oxygen atoms of phenyl ring. Lig65/ZINC25044394 form van der Waals interaction with Asp539, which is involved in the hbond interaction of native ligand of x-ray pose. Figure 5 displays the binding modes of each hit molecules into the active site of BTK.

In order to investigate the stabilities of docked complexes, molecular dynamics simulation was conducted for 100 ns. The root-mean square deviation (RMSD) for heavy atoms of protein was plotted as depicted in figure 6 (left). It is evident from Figure 6 (left) that both complexes were very stable during 100 ns. The RMSD for Lig65 complex was slightly higher as compared with that of 2V3, however, the values of both were under 2Å, which indicated their stabilities. On the other hand, protein residue flexibility was analyzed by the root mean square fluctuation (RMSF) values as depicted in figure 6 (right). It is shown that the protein residues were stable enough in both complexes. Higher values of RMSFs were observed in loop regions of protein, however, they are still acceptable considering their fluctuation was under 4 Å.

Further, in order to evaluate the affinities of docked ligands, binding energies were computed according to MM-PBSA method, which is considered more accurate in binding energy prediction as compared to docking method.

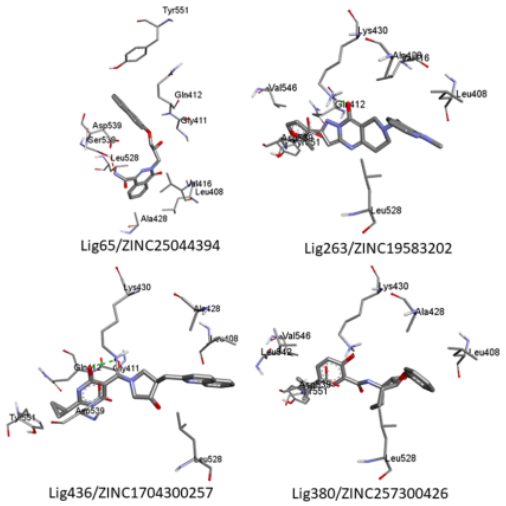

Figure 5. The docked poses of Lig65/ZINC25044394, Lig263/ZINC19583202, Lig436/ZINC1704300257, and Lig380/ZINC257300426, each in the active pocket of BTK.

As shown in Table 3, binding energy of 2V3 (−33.07±7.99 kcal/mol) was lower than that of Lig65 (−21.96±2.12). Binding interactions were supported by advantageous electrostatic (ΔE_{ELE}), van der Waals (ΔE_{VDW}), and non-polar energies of desolvation (ΔE_{PBSUR}). While that of polar energy of desolvation (ΔE_{PBCAL}) opposed the interaction in both complexes.

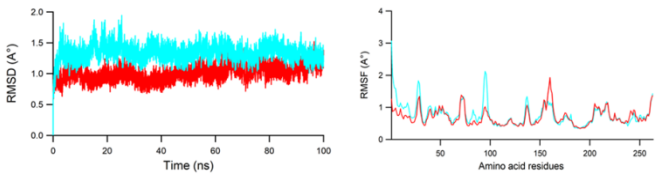

Figure 6. Plots representing RMSD profile of heavy atoms of protein (left) and RMSF profile of BTK (right), in which 2V3 and Lig65 were colored as red and blue, respectively.

4. CONCLUSIONS

In summary, a reliable structure-based pharmacophore model was generated based on the interaction of 2V3 with BTK. Using the pharmacophore model, 1337 molecules were identified as potential BTK inhibitors. The identified molecules were docked to BTK to reveal their mode of interaction. Four top docked ligands were revealed to interacted with BTK in the active site, which was further confirmed by the RMSD and RMSF plots of 100 MD simulation to afford one best hit. The binding affinity of the hit molecule was comparable with that of 2V3, which suggested the need for further experimental verification.

5. REFERENCES

1. Zou, Y.; Xiao, J.; Tu, Z.; Zhang, Y.; Yao, K.; Luo, M.; Ding, K.; Zhang, Y.; Lai, Y. Structure-Based Discovery of Novel 4,5,6-Trisubstituted Pyrimidines as Potent Covalent Bruton's Tyrosine Kinase Inhibitors. *Bioorganic Med Chem Lett* **2016**, *26*, 3052–3059, https://doi.org/10.1016/j.bmcl.2016.05.014.
2. Young, W.B.; Barbosa, J.; Blomgren, P.; Bremer, M.C.; Crawford, J.J.; Dambach, D.; Eigenbrot, C.; Gallion, S.; Johnson, A.R.; Kropf, J.E.; Lee, S.H.; Liu, L.; Liu, L.; Lubach, J.W.; Macaluso, J.; Maciejewski, P.; Mitchell, S.A.; Ortwine, D.F.; Di Paolo, J.; Reif, K.; Scheerens, H.; Schmitt, A.; Wang, X.; Wong, H.; Xiong, J.M.; Xu, J.; Yu, C.; Zhao, Z.; Currie, K.S. Discovery of Highly Potent and Selective Bruton's Tyrosine Kinase Inhibitors: Pyridazinone Analogs with Improved Metabolic Stability. *Bioorganic Med Chem Lett* **2016**, *26*, 575–579, https://doi.org/10.1016/j.bmcl.2015.11.076.
3. Shi, Q.; Tebben, A.; Dyckman, A.J.; Li, H.; Liu, C.; Lin, J.; Spergel, S.; Burke, J.R.; McIntyre, K.W.; Olini, G.C.; Strnad, J.; Surti, N.; Muckelbauer, J.K.; Chang, C.; An, Y.; Cheng, L.; Ruan, Q.; Leftheris, K.; Carter, P.H.; Tino, J.; De Lucca, G.V. Purine Derivatives as Potent Bruton's Tyrosine Kinase (BTK) Inhibitors for Autoimmune Diseases. *Bioorganic Med Chem Lett* **2014**, *24*, 2206–2211, https://doi.org/10.1016/j.bmcl.2014.02.075.
4. Gao, X.; Wang, J.; Liu, J.; Guiadeen, D.; Krikorian, A.; Boga, S.B.; Alhassan, A.B.; Selyutin, O.; Yu, W.; Yu, Y.; Anand, R.; Liu, S.; Yang, C.; Wu, H.; Cai, J.; Cooper, A.; Zhu, H.; Maloney, K.; Gao, Y.D.; Fischmann, T.O.; Presland, J.; Mansueto, M.; Xu, Z.; Leccese, E.; Zhang-Hoover, J.; Knemeyer, I.; Garlisi, C.G.; Bays, N.; Stivers, P.; Brandish, P.E.; Hicks, A.; Kim, R.; Kozlowski, J.A. Discovery of Novel BTK Inhibitors with Carboxylic Acids. *Bioorganic Med Chem Lett* **2017**, *27*, 1471–1477, https://doi.org/10.1016/j.bmcl.2016.11.079.
5. Huang, Z.; Zhang, Q.; Yan, L.; Zhong, G.; Zhang, L.; Tan, X.; Wang, Y. Approaching the Active Conformation of 1,3-Diaminopyrimidine Based Covalent Inhibitors of Bruton's Tyrosine Kinase for Treatment of Rheumatoid Arthritis. *Bioorganic Med Chem Lett* **2016**, *26*, 1954–1957, https://doi.org/10.1016/j.bmcl.2016.03.011.
6. Foluso, O.; Glick, A.; Stender, M.; Jaiyesimi, I. Ibrutinib as a Bruton Kinase Inhibitor in the Management of Chronic Lymphocytic Leukemia: A New Agent with Great Promise. *Clin Lymphoma, Myeloma Leuk* **2016**, *16*, 63–69, https://doi.org/10.1016/j.clml.2015.11.011.
7. Wu, J.; Zhang, M.; Liu, D. Bruton Tyrosine Kinase Inhibitor ONO/GS-4059: From Bench to Bedside. *Oncotarget* **2017**, *8*, 7201–7207, https://doi.org/10.18632/oncotarget.12786.
8. Ge, Y.; Yang, H.; Wang, C.; Meng, Q.; Li, L.; Sun, H.; Zhen, Y.; Liu, K.; Li, Y.; Ma, X. Design and Synthesis of Phosphoryl-Substituted Diphenylpyrimidines (Pho-DPPYs) as Potent Bruton's Tyrosine Kinase (BTK) Inhibitors: Targeted Treatment of B Lymphoblastic Leukemia Cell Lines. *Bioorganic Med Chem* **2017**, *25*, 765–772, https://doi.org/10.1016/j.bmc.2016.11.054.
9. Zhao, D.; Huang, S.; Qu, M.; Wang, C.; Liu, Z.; Li, Z.; Peng, J.; Liu, K.; Li, Y.; Ma, X.; Shu, X. Structural Optimization of Diphenylpyrimidine Derivatives (DPPYs) as Potent Bruton's Tyrosine Kinase (BTK) Inhibitors with Improved Activity toward B Leukemia Cell Lines. *Eur J Med Chem* **2017**, *126*, 444–455, https://doi.org/10.1016/j.ejmech.2016.11.047.
10. Zhao, X.; Xin, M.; Huang, W.; Ren, Y.; Jin, Q.; Tang, F.; Jiang, H.; Wang, Y.; Yang, J.; Mo, S.; Xiang, H. Design, Synthesis and Evaluation of Novel 5-Phenylpyridin-2(1H)-One Derivatives as Potent Reversible Bruton's Tyrosine Kinase Inhibitors. *Bioorganic Med Chem* **2015**, *23*, 348–364, https://doi.org/10.1016/j.bmc.2014.11.006.
11. Fioressi, S.E.; Bacelo, D.E.; Duchowicz, P.R. QSAR Study of Human Epidermal Growth Factor Receptor (EGFR) Inhibitors: Conformation-Independent Models. *Med Chem Res*, **2019**, *28*, 2079–2087, https://doi.org/10.1007/s00044-019-02437-y.
12. Wolber, G.; Langer, T. LigandScout: 3-D Pharmacophores Derived from Protein-Bound Ligands and Their Use as Virtual Screening Filters. *J Chem Inf Model* **2005**, *45*, 160–169, https://doi.org/10.1021/ci049885e.
13. Lou, Y.; Han, X.; Kuglstatter, A.; Kondru, R. K.; Sweeney, Z. K.; Soth, M.; McIntosh, J.; Litman, R.; Suh, J.; Kocer, B.; Davis, D.; Park, J.; Frauchiger, S.; Dewdney, N.; Zecic, H.; Taygerly, J.P.; Sarma, K.; Hong, J.; Hill, R.J.; Gabriel, T.; Goldstein, D.M.; Owens, T.D. Structure-Based Drug Design of RN486, a Potent and Selective Bruton's Tyrosine Kinase (BTK) Inhibitor, for the Treatment of Rheumatoid Arthritis. *J Med Chem* **2015**, *58*, 512–516, https://doi.org/10.1021/jm500305p.
14. Mysinger, M.M.; Carchia, M.; Irwin, J.J.; Shoichet, B.K. Directory of Useful Decoys, Enhanced (DUD-E): Better Ligands and Decoys for Better Benchmarking. *J Med Chem* **2012**, *55*, 6582–6594, https://doi.org/10.1021/jm300687e.
15. Sunseri, J.; Koes, D.R. Pharmit: Interactive Exploration of Chemical Space. *Nucleic Acids Res* **2016**, *44*, W442–W448, https://doi.org/10.1093/nar/gkw287.
16. Morris, G. M.; Huey, R.; Lindstrom, W.; Sanner, M.F.; Belew, R.K.; Goodsell, D.S.; Olson, A.J. AutoDock4 and AutoDockTools4: Automated Docking with Selective Receptor Flexibility. *J Comput Chem* **2009**, *30*, 2785–2791,

https://doi.org/10.1002/jcc.21256.
17. Maier, J.A.; Martinez, C.; Kasavajhala, K.; Wickstrom, L.; Hauser, K.E.; Simmerling, C. Ff14SB: Improving the Accuracy of Protein Side Chain and Backbone Parameters from Ff99SB. *J Chem Theory Comput* **2015**, *11*, https://doi.org/10.1021/acs.jctc.5b00255.
18. Wang, J.M.; Wolf, R.M.; Caldwell, J.W.; Kollman, P.A.; Case, D.A. Development and Testing of a General Amber Force Field. *J Comput Chem* **2004**, *25*, 1157–1174, https://doi.org/10.1002/jcc.20035.
19. Jakalian, A.; Jack, D.B.; Bayly, C.I. Fast, Efficient Generation of High-Quality Atomic Charges. AM1-BCC Model: II. Parameterization and Validation. *J Comput Chem* **2002**, *23,* 1623–1641, https://doi.org/10.1002/jcc.10128.
20. Arba, M.; Nur-Hidayat, A.; Surantaadmaja, S.I.; Tjahjono, D.H. Pharmacophore-Based Virtual Screening for Identifying B5 Subunit Inhibitor of 20S Proteasome. *Comput Biol Chem* **2018**, *77*, 64–71, https://doi.org/10.1016/j.compbiolchem.2018.08.009.
21. Ryckaert, J.P.; Ciccotti, G.; Berendsen, H.J.C. Numerical Integration of the Cartesian Equations of Motion of a System with Constraints: Molecular Dynamics of n-Alkanes. *J Comput Phys* **1977**, *23*, 327–341, https://doi.org/10.1016/0021-9991(77)90098-5.
22. Darden, T.; York, D.; Pedersen, L. Particle Mesh Ewald: An N·log(N) Method for Ewald Sums in Large Systems. *The Journal of Chemical Physics* **1993**, *98*, 10089–10092, https://doi.org/10.1063/1.464397.
23. Roe, D.R.; Cheatham III, T.E. PTRAJ and CPPTRAJ: Software for Processing and Analysis of Molecular Synamics Trajectory Data. *J Chem Theory Com* **2013**, *9*, 3084–3095, https://doi.org/10.1021/ct400341p.
24. Humphrey, W.; Dalke, A.; Schulten, K. VMD: Visual Molecular Dynamics. *Journal of Molecular Graphics* **1996**, *14,* 33–38, https://doi.org/10.1016/0263-7855(96)00018-5.
25. Arba, M.; Nurmawati, O. Identification of Phosphatidylinositol 3-Kinase δ (PI3Kδ) Inhibitor: Pharmacophore-Based Virtual Screening and Molecular Dynamics Simulation. *Indones J Chem* (accepted).
26. Braga, R.C.; Andrade, C.H. Assessing the Performance of 3D Pharmacophore Models in Virtual Screening: How Good Are They? *Curr Top Med Chem* **2013**, *13*, 1127–1138, https://doi.org/10.2174/15680266113130900010.

6. ACKNOWLEDGEMENTS

MA acknowledge the Ministry of Research and Technology, Republic of Indonesia, for funding this research.